ISSN NO. 2320-5407

Journal homepage: http://www.journalijar.com

INTERNATIONAL JOURNAL OF ADVANCED RESEARCH

RESEARCH ARTICLE

Necessity of Strain Hardening to Augment Load Bearing Capacity of AA1050/AlN Nanocomposites

A. Chennakesava Reddy

Department of Mechanical Engineering, JNTUH College of Engineering, Kukatpally, Hyderabad, India.

Manuscript Info

Manuscript History:

Received: 14 April 2015
Final Accepted: 21 May 2015
Published Online: June 2015

Key words:

RVE models, AlN, AA1050, finite lement analysis, interphase, nanocomposite.

Corresponding Author

A. Chennakesava Reddy

Abstract

In this article two types of RVE models have been implemented using finite element analysis. Aluminum nitride (AlN) nanoparticles were used as a reinforcing material in the matrix of AA1050 aluminum alloy. It has been observed that the nanoparticle did not overload during the transfer of load from the matrix to the nanoparticle due to interphase between the nanoparticle and the matrix. The tensile strength has been found increasing with change of strain hardening process from H-14 to H-18. The stress concentrations were found to be low in the nanocomposites having interphase between the matrix and the nanoparticle. The load bearing ability has been found increased as the interphase became stiffer with change of strain hardening process form H-14 to H-18.

INTRODUCTION

For composite materials, the aluminum nitride (AlN) nanoparticles have good interface compatibility, and can improve the mechanical properties of composite materials and the thermal conductivity of dielectric. AlN is used for manufacturing integrated circuit board, electronic devices, optical devices, radiator, and high temperature crucible; for fabrication of metal matrix and polymer matrix composites, especially in the heat seal adhesives and electronic packaging materials and high thermally conductive ceramics.

1050 aluminum alloy is commonly used in the electrical and chemical industries, on account of having high electrical conductivity, corrosion resistance, and workability. It has low mechanical strength compared to more significantly alloyed metals. This is a non-heat treatable aluminum alloy. A heat-treatment of this alloy does not produce any strengthening precipitates as in the heat treatable alloys. The strength may in fact decrease during heat treatment due to the removal of solute atoms.

The higher stiffness of ceramic particles can lead to an incremental increase in the stiffness of a composite (Chennakesava and Essa Zitoun, 2011). Micron-sized particles usually cause a reduction in impact resistance. On the other hand, using nanoparticles can lead to better impact and wear performance (Friedrich et al, 2005). The existence of an interphase region with a higher strength and modulus than the polymer matrix would cause the composites to have superior mechanical properties (Romanowicz, 2010). Decreasing the interfacial strength can cause the interfacial debonding of particles from the matrix. Interfacial debonding can cause shear yielding of the matrix around the particles. Very small particles are difficult to disperse, creating agglomerates that behave as a large, single particle (Thio, 2002). The tensile properties of nanocomposites, including their tensile strength and elastic modulus, were analyzed via micromechanical models. The modulus magnitude depends on interfacial adhesion and the matrix's crystalline structure (Wang, 2003; Chennakesava, 2004).

The finite element procedure and analytical methods have been exceptionally effective in determining the mechanical properties of non-homogeneous materials like composites. In finite element numerical models very fine meshes need to be applied inside and around the interphase layers which results in large number of degrees of

freedom. Currently, the use of a representative volume element (RVE) or a unit cell of the composite microstructure, in conjunction with a finite element (FE) analysis tool is well established for examining the effective material properties and understanding the micromechanics of the composite materials.

AA1050 aluminum alloy can be strengthened by cold working, but not by heat treatment. The purpose of this paper is to enhance the load bearing ability of AA1050/AlN nanocomposite by strain hardening.

1. Strengthening Mechanisms

The strength of a particulate metal matrix composite depends on the strength of the weakest zone and metallurgical phenomena in it (Chennakesava, 2011; Chennakesava and Kotiveerchari, 2011). For very strong particle-matrix interfacial bonding, a new criterion (Chennakesava, 2015) is suggested by the author considering adhesion, formation of precipitates, particle size, agglomeration, voids/porosity, obstacles to the dislocation, and the interfacial reaction of the particle/matrix. The formula for the strength of composite is stated below:

$$\sigma_c = \sigma_m \left[\frac{1-(v_p+v_v)^{2/3}}{1+2(v_p+v_v)}\right] e^{m_p(v_p+v_v)} + k d_p^{-1/2} \quad (1)$$

where v_v and v_p are the volume fractions of voids and particles respectively in the composite, m_m and m_p are the possion's ratios of the matrix and particulates, and k is $E_m m_m / E_p m_p$. E_m and E_p are elastic moduli of matrix and particles respectively; d_p is the average diameter of the particle.

Elastic modulus (Young's modulus) is a measure of the stiffness of a material and is a quantity used to characterize materials. Elastic modulus is the same in all orientations for isotropic materials. Anisotropy can be seen in many composites. The proposed equation by the author to find Young's modulus includes the effect of voids/porosity in the composite as given below:

$$\frac{E_c}{E_m} = \left(\frac{1-v_v^{2/3}}{1-v_v^{2/3}+v_v}\right)\left[\frac{1+(\delta-1)v_p^{2/3}}{1+(\delta-1)(v_p^{2/3}-v_p)}\right] \quad (2)$$

where, $\delta = E_p/E_m$.

2. Materials and Methods

The matrix material was AA1050 aluminum alloy. The reinforcement material was aluminum nitride (AlN) nanoparticles of average size 100nm. The mechanical properties of materials used in the present work are given in table 1.

3.1 Preparation of composite specimens

The matrix alloys and composites were prepared by the stir casting and low-pressure die casting process. The volume fractions of carbon black reinforcement were 10%, 20%, and 30%. AA1050 matrix alloy was melted in a resistance furnace. The crucibles were made of graphite. The melting losses of the alloy constituents were taken into account while preparing the charge. The charge was fluxed with coverall to prevent dressing. The molten alloy was degasified by tetrachlorethane (in solid form). The crucible was taken away from the furnace and treated with sodium modifier. Then the liquid melt was allowed to cool down just below the liquidus temperature to get the melt semi solid state. At this stage, the preheated (500^0C for 1 hour) reinforcement particles were added to the liquid melt. The molten alloy and reinforcement particles are thoroughly stirred manually for 15 minutes. After manual steering, the semi-solid, liquid melt was reheated, to a full liquid state in the resistance furnace followed by an automatic mechanical stirring using a mixer to make the melt homogenous for about 10 minutes at 200 rpm. The temperature of melted metal was measured using a dip type thermocouple. The preheated cast iron die was filled with dross-removed melt by the compressed (3.0 bar) argon gas (Chennakesava, 2015).

2.2 Strain hardening

Work hardening, also known as strain hardening or deformation hardening, is a phenomenon where the strength of a material increases during plastic deformation. The stir cast test samples were homogenized. For homogenization the test samples were heated at a constant rate of 100°C/h to 550°C, then held at 550°C for 6 hours, and slowly cooled at a rate of 6°C/h to a temperature of 350°C before quenching. The homogenized were cold rolled to get strain hardening conditions of H-14, H-16 and H-18 as shown in figure 1. AA1050/AlN nanocomposites were cold rolled

directly from as-cast and homogenized condition in a laboratory mill a relatively low strain rate, probably less than 1. Lubricated rolls were used at maximum speed. The strain was calculated from the thicknesses of the test samples before and after rolling process. The strain measurements are defined by:

$$\varepsilon = \ln \frac{t_o}{t} \quad (3)$$

where, to and t are thickness of the test sample before and after rolling.

2.3 Tensile testing

The heat-treated samples were machined to get flat-rectangular specimens (figure 2) for the tensile tests. The tensile specimens were placed in the grips of a Universal Test Machine (UTM) at a specified grip separation and pulled until failure. The test speed was 2 mm/min (as for ASTM D3039). A strain gauge was used to determine elongation as shown in figure 3.

3.4 Optical and scanning electron microscopic analysis

An image analyzer was used to study the distribution of the reinforcement particles within the AA1050 aluminum alloy matrix. The polished specimens were ringed with distilled water, and etched with 0.5% HF solution for optical microscopic analysis. Fracture surfaces of the deformed/fractured test samples were analyzed with a scanning electron microscope (SEM) to define the macroscopic fracture mode and to establish the microscopic mechanisms governing fracture. Samples for SEM observation were obtained from the tested specimens by sectioning parallel to the fracture surface and the scanning was carried using S-3000N Toshiba SEM.

3.5 RVE modeling using finite element analysis (FEA)

The representative volume element (RVE or the unit cell) is the smallest volume over which a measurement can be made that will yield a value representative of the whole. In this research, a cubical RVE was implemented to analyze the tensile behavior AA1050/AlN nanocomposites (figure 4). The determination of the RVE's dimensional conditions requires the establishment of a volumetric fraction of spherical nanoparticles in the composite. Hence, the weight fractions of the particles were converted to volume fractions. The volume fraction of a particle in the RVE is determined using equation (Hill, 1963):

$$v_p(\text{RVE}) = \frac{\text{Volume of nanoparticle}}{\text{Volum e of RVE}} = \frac{16}{3} \times \left(\frac{r}{a}\right)^3 \quad (4)$$

where, r represents the particle radius and a indicates the diameter of the cylindrical RVE. The volume fraction of the particles in the composite (V_p) was chosen to be 0.30 and the particle radius (r) was taken to be 50 nm.

The RVE dimension (a) was determined by equalizing equation (4). Two RVE schemes namely: without interphase (adhesion) and with interphase were applied between the matrix and the filler. The loading on the RVE is defined as symmetric displacement, which provided equal displacements at both ends of the RVE. To obtain the nanocomposite modulus and yield strength, the force reaction is defined against displacement. The large strain PLANE183 element was used in the matrix and the interphase regions in all the models (table 2). In order to model the adhesion between the interphase and the particle, a COMBIN14 spring-damper element was used. The stiffness of this element was taken as unity for perfect bonding which determines the interfacial strength for the interface region.

To converge an exact nonlinear solution, it is also important to set the strain rates of the FEM models based on the experimental tensile tests' setups. Hence, FEM models of different RVEs with various particle contents should have comparable error values. In this respect, the ratio of the tensile test speed to the gauge length of the specimens should be equal to the corresponding ratio in the RVE displacement model. Therefore, the rate of displacement in the RVEs was set to be 1.0 (1/min).

3. Results and Discussion

Figure 5 reveals the microstructure of AA1050/AlN nanocomposite. The AlN nanoparticles are randomly distributed in the AA1050 matrix. Figure 6 depicts the tensile strengths of the nanocomposites obtained by FEA (RVE model), AC Reddy model, and experimental procedure. The tensile strength increases with change in the strain hardening process from H-14 to H-18.

Without interphase and barely consideration of adhesive bonding, the debonding occurs at the particle/matrix interface region in the nanocomposite as shown in figure 7. It is also observed that the stress induced in the nanoparticle gets increased with change in the strain hardening process from H-14 to H-18. This indicates the load bearing capacity increases with change in the strain hardening process from H-14 to H-18. Figure 8 shows the effect of interphase between the nanoparticle and the matrix on the stress induced in the nanocomposite in the direction of tensile loading. In the composite there is an evidence of breakage of bonding not only between the nanoparticle and the interphase but also between the matrix and the interphase.

Author's model includes the effect of voids present in the nanocomposite. In the presence of voids in the nanocomposite, the interface region between the nanoparticle and the matrix gets stiffened and consequently this leads the slow rate of increasing (or remain constant) the tensile strength with an increase in the nanoparticles content. The results obtained from Author's model were nearly equal to the experimental values. On the other hand, the deviation of FEA (RVE model) results with the experimental results possibly occurs as a result of micro-metallurgical factors (such as formation of voids and nanoparticle clustering) that were not considered in the RVE models. However, the nonlinear deformation behavior of the reinforcements and the matrix/reinforcement debonding were considered in the RVE models. These micromechanical factors might be important in the large plastic deformation regime.

Figure 9 shows the tensile strain contours of the RVE models for the situation involving without interphase. Figure 10 shows the tensile strain contours of the RVE models for the situation involving with interphase. According to figure 9 and 10, the RVE is expanded elastically away from the particle in the direction of the tensile loading. This increases the contact area between the particle and the matrix in the perpendicular direction to the tensile loading and decreases the contact area between the particle and the matrix in the direction of the tensile loading. In addition, the deformation is propagated in the normal direction to the tensile loading. It is also observed that the strain induced is higher in the nanocomposites having interphase between the matrix and the nanoparticle than that induced in the nanocomposites without interphase. This is on account of the additional elongation of interphase before it debonds with nanoparticle and the matrix.

Table 3 gives the elastic (tensile) moduli of the nanocomposites obtained by the Rule of Mixtures, and Author's model. The results provided by Author's model were higher than the results obtained by the Rule of Mixture. This is due to the metallurgical phenomenon such as voids, clustering of nanoparticles in the nanocomposites.

Figure 11 shows the variation of von Mises stress in the nanocomposite without interphase. The von Mises stress increases with strain hardening process from H-14 to H-18. The adhesion strength at the interface determines the load transfer between the components. Effective stress transfer is the most important factor which contributes to the strength of two-phase composite materials. Discontinuity in the form of debonding exists because of non-adherence of particle to matrix. However, for strain hardened nanocomposites, enhancement of nanoparticle adhesion to the matrix will lead to an increase in strength especially for nanoparticles with high surface areas. It is observed from figure 10 that the debonding occurs at the entire periphery of the nano particle without interphase between the nanoparticle and the matrix. Hence, the stress transfer from the matrix to the nanoparticle becomes less for the nanocomposites without interphase. It is noticed from figure 12 that the debonding occurs at the partial periphery of the nanoparticle with interphase between the nanoparticle and the matrix. Hence, the stress transfer from the matrix to the nanoparticle becomes high for the nanocomposites with interphase. In the case of nanocomposites with interphase between the nanoparticle and the matrix, the stress is transferred through shear from the matrix to the particles. The stress contours are appearing same in all the strain hardening processes because the elastic modulus of the matrix is same in all the cases. The only difference is the loading bearing capacity which increases with strain hardening process from H-14 to H-18.

The stress concentration around the nanoparticle without interphase can be observed from figure 13. The stress concentration around the nanoparticle with interphase can be observed from figure 14. The stress concentration is higher in the nanocomposites without interphase between the matrix and the nanoparticle than in the nanocomposites with interphase between the matrix and nanoparticle. It is observed that the interfacial debonding is high between the particle and the matrix because of high local stress concentration around the nanoparticle in the nanocomposites without interphase. The plastic flows are initiated within the matrix and ended at the nanoparticle/matrix interface. Owing to the high stress of the nanoparticles, the plastic deformation becomes concentrated at several locations in the matrix. The localized strain is observed around the particle because of the high load-transfer effect in particles. The plastic behavior differs considerably with inclusion of interphase between the nanoparticle and the matrix. As the pressure is increased on the RVE model, the plastic strain zone expanded, resulting in a plastic deformation of the interphase between the nanoparticle and the matrix. In the present work the

interphase is softer than the matrix and the nanoparticle and the nano particle is stiffer than the matrix. The elastic moduli (stiffness) of AlN nanoparticle and AA1050 matrix are 330 GPa and 69 GPa respectively.

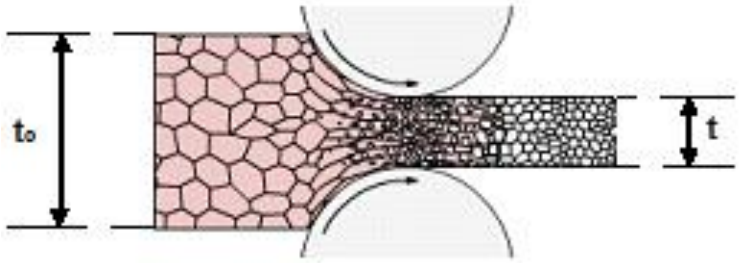

Figure 1: Strain hardening using rolling process

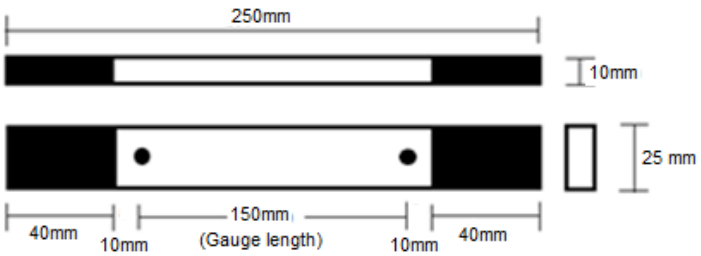

Figure 2: Shape and dimensions of tensile specimen.

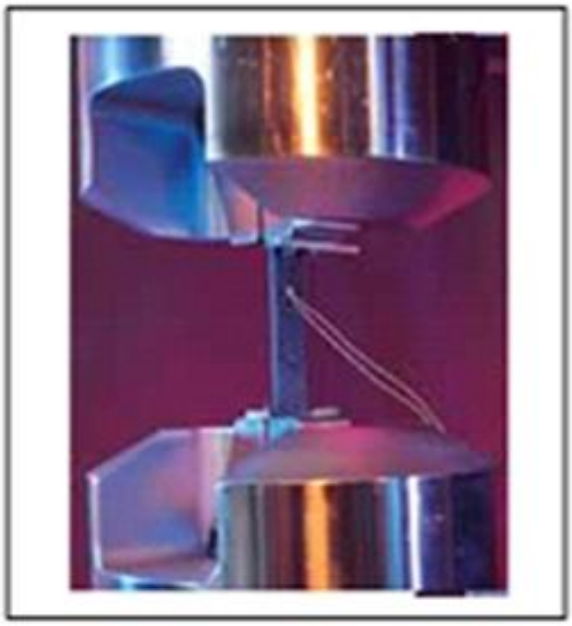

Figure 3: Tensile testing

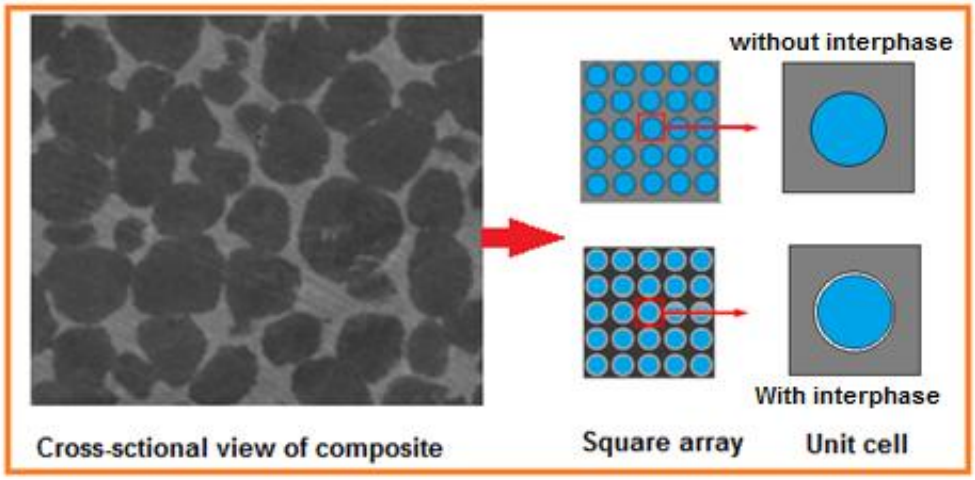

Figure 4: The RVE model.

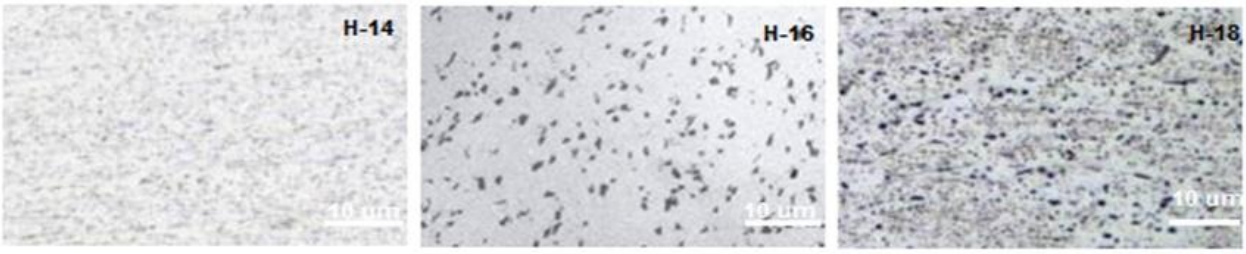

Figure 5: Optical microstructure of strain hardened AA1050/AlN nanocomposites.

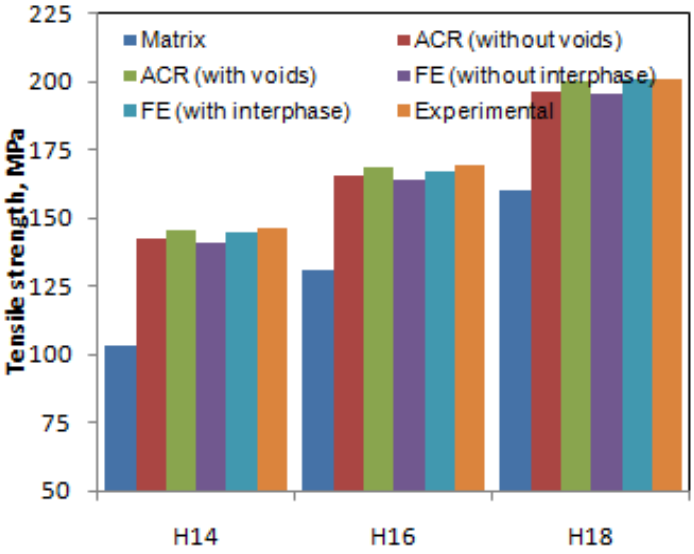

Figure 6: Effect of strain hardening on tensile strength.

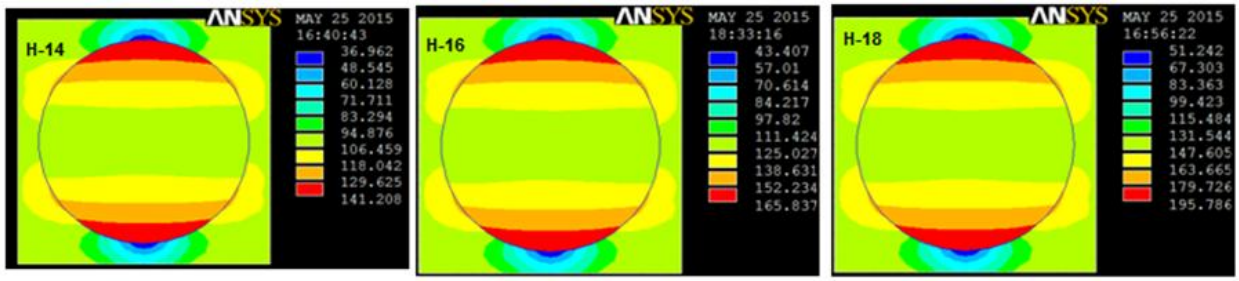

Figure 7: Tensile strength along load direction without interphase.

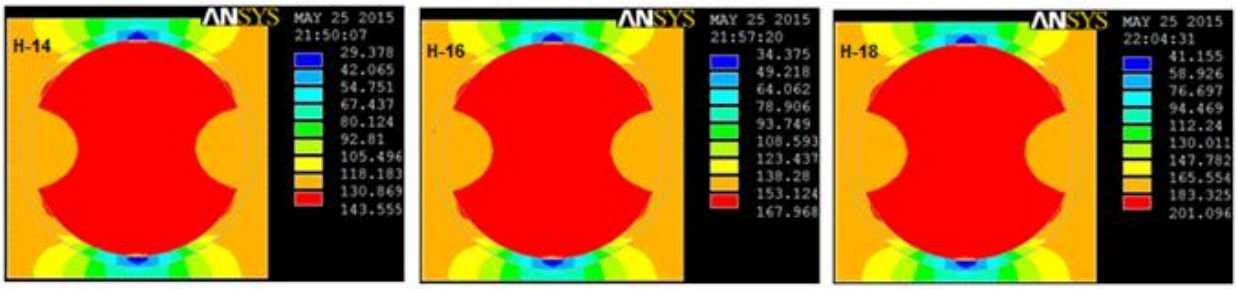

Figure 8: Tensile strength along load direction with interphase.

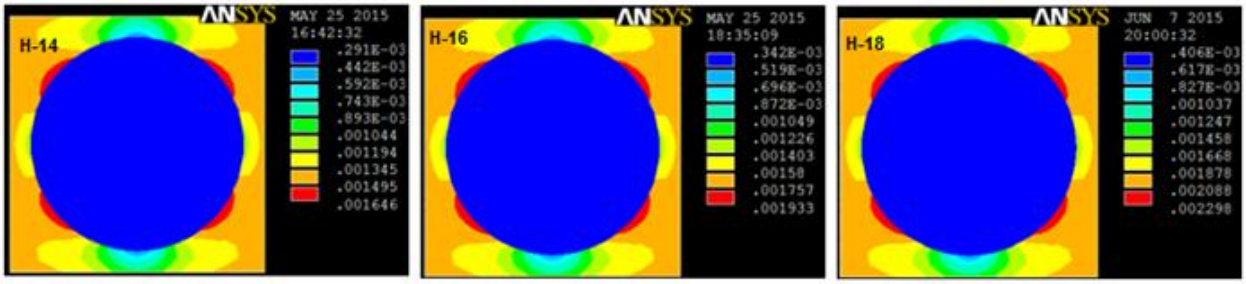

Figure 9: Tensile strain along load direction without interphase.

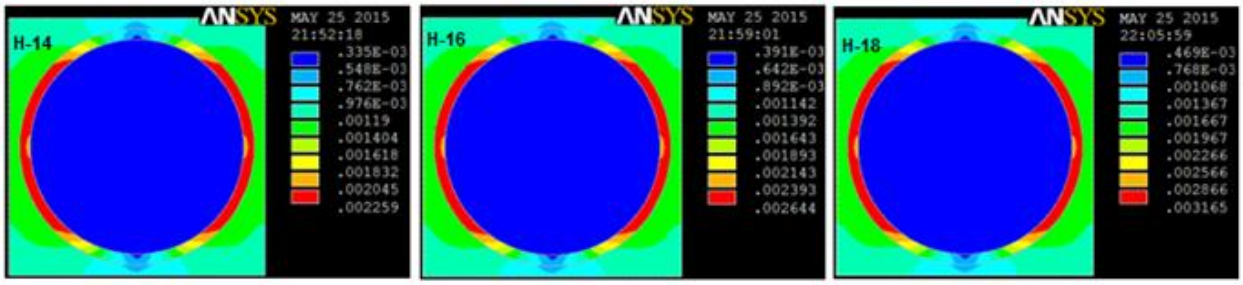

Figure 10: Tensile strain along load direction with interphase

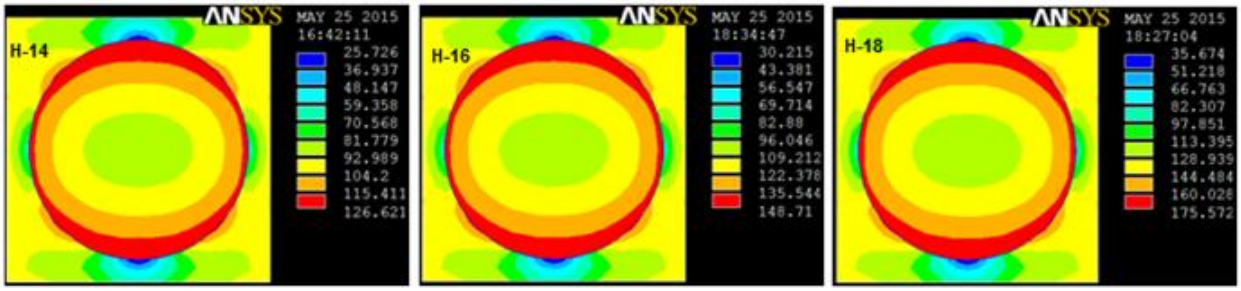

Figure 11: von Mises stress without interphase.

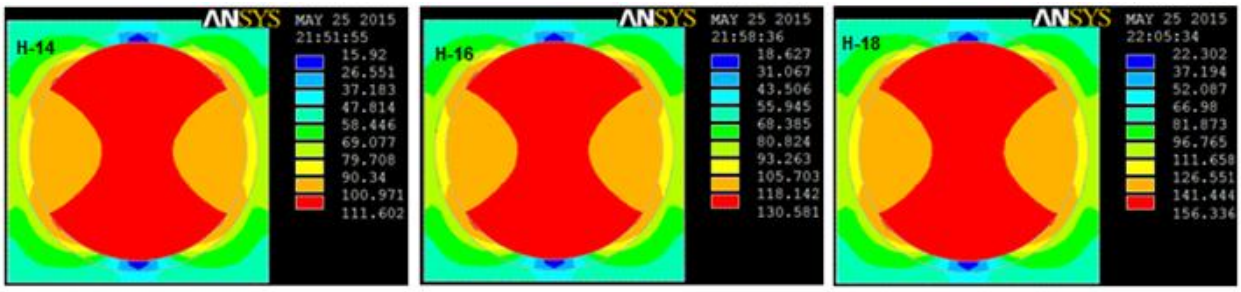

Figure 12: von Mises stress with interphase.

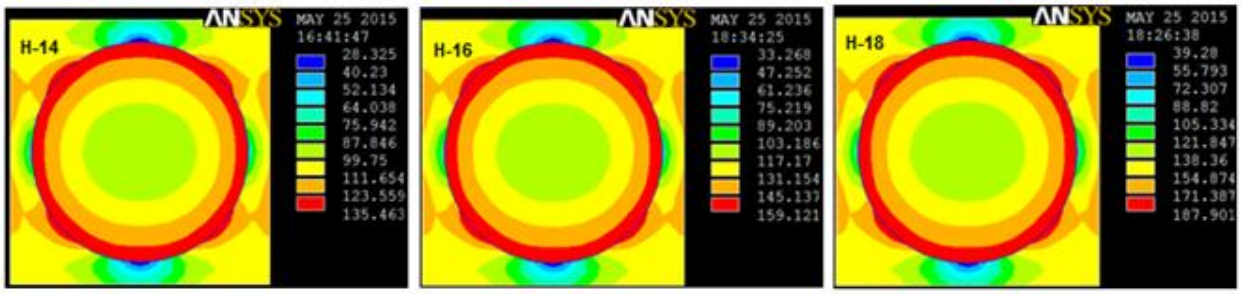

Figure 13: Stress intensity without interphase.

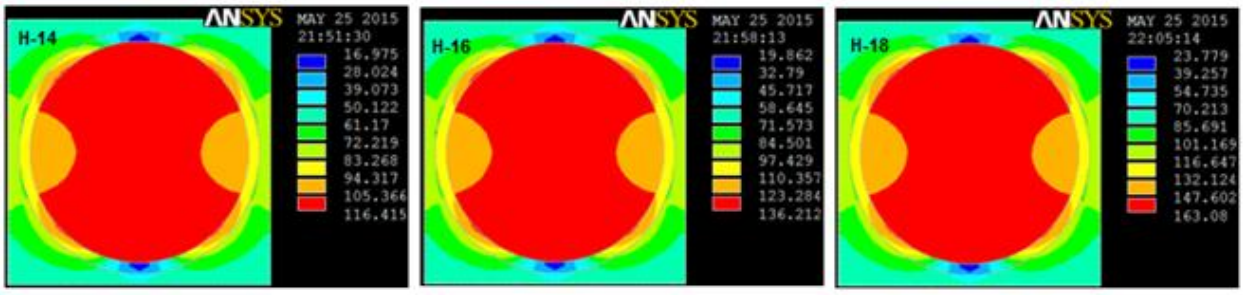

Figure 14: Stress intensity with interphase.

Table 1: Mechanical properties of AA1050 matrix and AlN nanoparticles

Property	AA1050 –H14	AA1050–H16	AA1050 –H18	AlN
Density, g/cc	2.705	2.705	2.705	3.26
Elastic modulus, GPa	69	69	69	330
Ultimate tensile strength, MPa	110	131	160	270
Poisson's ratio	0.33	0.33	0.33	0.24

Table 2: Elements features, applications and size ranges used in RVE modeling

Element code	Plane 183	Contact 172	Combination 14	Target 169
Feature	Quadrilateral-8 nodes	Linear 3 node	Longitudinal spring-damper	Shape complexity
Application	Matrix and interphase	Interface contact	Elastic modeling of adhesion	Contact bodies

Table 3: Elastic modulus obtained from models

Model	Elastic modulus, GPa
Rule of Mixture	97.80
AC Reddy	119.18

4. Conclusion

Without interphase and barely consideration of adhesive bonding, the debonding occurs at the particle/matrix interface region in the nanocomposite. Due to interphase between the nanoparticle and the matrix, the nanoparticle is not overloaded during the transfer of load from the matrix to the nanoparticle via the interphase. The tensile strengths obtained by AC Reddy model (with voids) and experimental results were nearly equal. In the case of nanocomposites with interphase between the nanoparticle and the matrix, the stress concentration is low around the nanoparticles. The tensile strength increases with change of strain hardening process from H-14 to H-18 for the AA1050/AlN nanocomposites.

Chennakesava Reddy, A. (2004). Analysis of the Relationship Between the Interface Structure and the Strength of Carbon-Aluminum Composites, NATCON-ME, Bangalore, 61-62.

Chennakesava Reddy, A. and Essa Zitoun. (2011). Tensile properties and fracture behavior of 6061/Al_2O_3 metal matrix composites fabricated by low pressure die casting process, International J. Mater. Sci. 6:147-157.

Chennakesava Reddy, A. (2011). Influence of strain rate and temperature on superplastic behavior of sinter forged Al6061/SiC metal matrix composites. Int. J. Eng. Res. & Technol. 4:189-198.

Chennakesava Reddy, A., and Kotiveerachari, B. (2011). Influence of microstructural changes caused by ageing on wear behaviour of Al6061/SiC composites. J. Metall. & Mater. Sci. 53:31-39.

Chennakesava Reddy, A. (2015). Influence of Particle Size, Precipitates, Particle Cracking, Porosity and Clustering of Particles on Tensile Strength of 6061/SiCp Metal Matrix Composites and Validation Using FEA. Int. J. Mater. Sci. and Manuf. Eng. 42:1176-1186.

Friedrich, K., Zhang, Z., Schlarb, A.K. (2005). Effects of various fillers on the sliding wear of polymer composites. Compo. Sci. Technol. 65:2329-2343.

Hill, R. (1963). Elastic properties of reinforced solids: some theoretical principles. J. of Mecha. and Phy. of Solids.11.

Romanowicz, M. (2010). Progressive failure analysis of unidirectional fiber-reinforced polymers with inhomogeneous interphase and randomly distributed fibers under transverse tensile loading. Composites part A. 41:1829-1838.

Thio, Y.S., Argon, A.S., Cohen, R.E., Weinberg, M. (2002). Toughening of Isotactic Polypropylene with CaCO3 Particles. Polymer. 43:3661-3674.

Wang, K., Wu, J., Ye, L., Zeng, H. (2003). Mechanical properties and toughening mechanisms of polypropylene/barium sulfate composites. Composites: Part A. 34:1199-1205.